Widespread permafrost thaw during Marine Isotope Stages 11 and 13 recorded by speleothems

Author: Nicole Brooke Biller

Boston College Electronic Thesis or Dissertation, 2017

WIDESPREAD PERMAFROST THAW DURING MARINE ISOTOPE STAGES 11 AND 13 RECORDED BY SPELEOTHEMS

Nicole B. Biller

A thesis

Submitted to the Faculty of

the department of Earth and Environmental Sciences

in partial fulfillment

of the requirements for the degree of

Master of Science

Boston College
Morrissey College of Arts and Sciences
Graduate School

December 2017

WIDESPREAD PERMAFROST THAW DURING MARINE ISOTOPE STAGES 11 AND 13 RECORDED BY SPELEOTHEMS

Nicole B. Biller

Advisor: Jeremy D. Shakun, Ph.D.

Abstract

Arctic permafrost contains a substantial stock of carbon that could be released to the atmosphere as CH_4 and CO_2 upon thawing, making it a potentially powerful amplifier of future warming. The sensitivity of permafrost to climate change is uncertain, however, and occurs on time scales longer than those captured by the instrumental record. Speleothems – cave precipitates deposited from flowing or dripping water – in currently frozen regions record past episodes of thaw, which can be used to assess the response of permafrost to long-term warmth. Here, we present 90 uranium-thorium ages on speleothems from across the North American Arctic, sub-Arctic and northern alpine regions to reconstruct a 600-kyr permafrost history. Widespread speleothem growth supports an episode of extensive permafrost thaw during the Marine Isotope Stage 11 interglacial about 400 ka, when global temperature was only slightly warmer than pre-industrial conditions. Additional growth is evident during MIS 13, curiously, a smaller magnitude interglacial. Ice-core records of atmospheric greenhouse gases do not show elevated concentrations at these times, perhaps suggesting that the permafrost carbon pool was smaller than today or released gradually enough to be buffered by other reservoirs.

Table of Contents

List of Tables

List of Figures

Introduction

Permafrost, or permanently frozen ground, is widespread in the Arctic and covers nearly a quarter of Northern Hemisphere land. It is typically categorized in zones based on the fraction of an area it covers – continuous (>90%), discontinuous (50-90%), sporadic (10-50%), and isolated (<10%) – and which roughly track climatic variations with latitude and elevation (French, 1999). Permafrost has warmed significantly over the past few decades (Romanovsky et al., 2010), and it may be highly vulnerable to thaw with continued climate change (Schuur et al., 2015). This trend has potential global implications because Arctic permafrost is estimated to contain ~1500 gigatons of carbon (Tarnocai et al., 2009) – twice as much as the atmosphere – which may be released as methane (CH_4) and carbon dioxide (CO_2) upon thawing. However, because the response of permafrost to climate change is mediated by a complex array of factors (e.g., ground cover, soil moisture, seasonality), models exhibit considerable disagreement on the amount of near-surface (0-3.5 m depth) permafrost loss expected with 21st century warming (Slater and Lawrence, 2013), from 2-66% in a low-emission scenario (RCP2.6) to 30-99% in the highest-emission scenario (RCP8.5) (Koven et al., 2013). Furthermore, a sizeable fraction of permafrost carbon exists below 3.5 m depth (Schuur et al., 2015), and likely responds on longer time scales.

An alternative way to assess the vulnerability of permafrost to warming is to reconstruct its stability during previous interglacial periods. While repeated glaciations have scraped away the surface evidence of pre-Holocene permafrost conditions in many northern areas, caves provide sheltered environments that can preserve long archives of paleoenvironmental information in these regions. In particular, the precipitation of calcite speleothems is currently limited in caves in permafrost regions due to lack of liquid water, reduced temperature, minimal soil productivity to charge groundwater with the necessary CO_2, and/or poor cave ventilation associated with ice plugs (Dreybrodt 1988, 1999); thus, speleothems in these locations are often relicts of past periods of thaw that enabled meteoric waters to seep into caves and deposit calcite (Lauriol et al., 1997; Vaks et al., 2013) (Supplementary Fig. 1). Other factors could also prevent speleothem growth locally despite thawed conditions, such as drought, high cave air CO_2, or organic carbon inhibiting calcite deposition (Fairchild and Baker, 2012; Lebron and Suarez 1996), but the widespread presence or absence of speleothem growth across northern regions is likely controlled by permafrost. Importantly, speleothems can be precisely dated over the past 600 kyr with uranium-thorium (U-Th) geochronology using inductively coupled plasma mass spectrometry (ICP-MS) (Cheng et al., 2013).

Vaks et al. (2013) recently tested this approach with a north-south transect of caves in Siberia and confirmed that speleothem growth was limited to interglacials. Notably, one sample from their northernmost cave suggests an episode of thaw extending to the modern-day continuous permafrost zone during Marine Isotope Stage 11 (MIS 11) about 400 kyr ago. On the other hand, a relict ice wedge underlying tephra from the discontinuous zone in the Yukon indicates that permafrost there has persisted for at least the past 740 kyr (Froese et al., 2008). Unfortunately, there are few long-term reconstructions from other areas to better evaluate these contrasting depictions of permafrost resilience to interglacial warming.

North American Speleothem Growth Chronology

Here we reconstruct past episodes of permafrost thaw in North American cold regions by measuring 90 U-Th ages on a collection of previously undated speleothems (n=64) obtained in the 1960s-90s from several regions of Alaska and Canada (Fig. 1). The sites cover a wide range of conditions, from isolated to continuous permafrost at 49 to 67˚N in alpine, sub-Arctic and Arctic settings, varying topographic relief, areas glaciated and never glaciated during the Pleistocene, and with caves of widely varying lengths and depths below the surface. Mean annual temperature in these regions ranges from -7˚C to slightly above freezing. The speleothems are predominantly small and often display sharp hiatuses, presumably reflecting limited and intermittent growth environments. Most samples are flowstones, with a smaller number of stalactites, popcorn, and stalagmites. Some were collected in situ, while others were found as broken formations on the cave floors. The Supplementary Information provides descriptions of each cave and sample and summary statistics.

Earlier U-Th dating at our sites using low-precision alpha spectrometry found that speleothem growth broadly clustered during late Pleistocene interglacials, while a substantial number of samples exceeded the dating limit of 350 ka (Harmon et al., 1977; Lauriol et al., 1997). Most significantly, the few speleothems (n=5) dated to <350 ka at our northernmost study area in the modern-day continuous zone were confined exclusively to cave entrances subject to the seasonal cycle, suggesting that the summer active layer may have thickened during recent interglacials but there was no major thaw (Lauriol et al., 1997). The speleothems we dated were not analyzed in these previous studies.

We dated the outermost laminae from each speleothem with ICP-MS to determine the youngest episode of growth, and obtained additional dates from stratigraphically older laminae on speleothems that were well within the analytical limits of the method. Except for a few (n=6) younger speleothems from the southern Canadian Rockies and one MIS 7 speleothem from a small rock shelter in the northern Yukon, all samples are >350 ka, and nearly half (n=32) exceed the U-Th limit of 600 ka (Fig. 2a). The fraction of infinite ages increases with latitude, a pattern also apparent in Siberian caves (Vaks et al., 2013) (Fig. 3c), which might imply that permafrost conditions have been more dominant at the northern locations for the past half million years. Uncertainties are relatively large on many of the finite ages (due to age and/or low U content), but they collectively show a prominent peak during MIS 11 and a secondary maximum associated with MIS 13. Bearing in mind the small number of samples, these ages exhibit notable geographic patterns, particularly when paired with the earlier alpha-spectrometric dating at these sites (Fig. 3a,b). In the southernmost region, peaks in the age distribution are similar between interglacials, perhaps suggesting comparable thaw every cycle. In contrast, the Nahanni caves in the discontinuous permafrost zone show an exceptional peak in speleothem deposition during MIS 11, while the northernmost Yukon caves show notable deposition during MIS 11 and especially MIS 13. We take these results to reflect widespread speleothem deposition and permafrost thaw across all of our sites during MIS 11, and an earlier episode of thaw during MIS 13.

Marine Isotope Stages 11 and 13

Although prior dating at these caves identified speleothem growth during younger interglacials (Harmon et al., 1977; Lauriol et al., 1997) (Fig. 3a), the speleothems we find from MIS 11 and 13 suggest that these interglacials were anomalous in the context of the past 600 kyr for several reasons. First, even if speleothems were deposited uniformly across interglacials, one would expect to find fewer of them from older interglacials because preservation decreases with age due to frost shattering, clastic infilling, dissolution, and retreat of cave entrances (Harmon et al., 1977; Lauriol et al., 1997; Scroxton et al., 2016) (Fig. 3b). Instead, however, the greatest number of speleothems date to MIS 11 in Nahanni (n=5) and MIS 13 in northern Yukon (n=9). Second, the few samples from younger interglacials in the continuous zone of northern Yukon are restricted to cave entrances that experience summer warmth. In contrast, we obtained multiple MIS 11 and 13 ages from the interior of the deepest cave in this area, where temperatures are constant year round and below zero, consistent with substantial thaw then. Lastly, while numerous site-specific factors control permafrost thaw and speleothem deposition, which may help explain some of the differences in the concentration of speleothem ages between regions, the replication of the MIS 11 and 13 signals in multiple caves from several of these areas suggests that they are robust. Furthermore, Vaks et al. (2013) also found that speleothem growth in the continuous zone of Siberia was limited to these two interglacials (Fig. 3c), suggesting that permafrost thaw may have spanned much of the Arctic at these times.

The widespread degradation of permafrost inferred during MIS 11 fits into a broader patchwork of Arctic climate records suggesting particularly strong warming during this interglacial, which was perhaps the most intense of the past 800 kyr (Harmon et al., 1977; Past Interglacials Working Group, 2016). Sea level was 6-13 m higher (Raymo and Mitrovica, 2012), Greenland was at least partially deglaciated (Reyes et al., 2014) and had boreal forests (Willerslev et al., 2007; de Vernal and Hillaire-Marcel, 2008) (Fig. 3d), the Arctic Ocean was seasonally ice free (Cronin et al., 2013), and summer temperatures were up to 5˚C above present at Lake El'gygytgyn in northeast Siberia (Melles et al., 2012). In contrast, widespread permafrost thaw during MIS 13 is more difficult to reconcile with most paleoclimate records, which typically suggest that it was a "luke-warm" interglacial, among the coolest of the past 800 kyr (Past Interglacials Working Group, 2016) (Fig. 3g). Two notable exceptions, however, both in the Arctic, are a spike in pollen deposition off of southern Greenland suggestive of ice sheet retreat there (de Vernal and Hillaire-Marcel, 2008) (Fig. 3d), and ostracode assemblages in the Arctic Ocean consistent with summer sea-ice loss (Cronin et al., 2013).

Why was the permafrost response during MIS 11 and 13 exceptional? MIS 11, and by some measures MIS 13, were unusually long interglacials (Past Interglacials Working Group, 2016), which could have provided sufficient time for warming to thaw permafrost, or melt the Greenland Ice Sheet and amplify Arctic warming. However, some of our North American and Vaks et al.'s (2013) Siberian speleothems grew near the onset of MIS 11 (Fig. 3a,c) precluding interglacial duration as the root cause of permafrost thawing. Orbital and greenhouse-gas forcings were similar to or weaker than the Holocene, and thus cannot explain the anomalous warmth (Fig. 3e,f). Modeling has identified some mechanisms that could exacerbate Arctic warming, such as vegetation-albedo feedback, enhanced oceanic heat transport through Arctic gateways due to higher sea level reducing sea ice, and reductions in the Greenland Ice Sheet (Melles et al., 2012). Nonetheless, the geographic reach and/or strength of these feedbacks may be too limited to explain strong pan-Arctic warmth (Melles et al., 2012). Moreover, these processes have largely been invoked to drive summer warming, and many of the proxies discussed above are seasonally biased toward summers. Thus, it is unclear how mean annual temperature, the first-order control on cave temperature, might have changed during past interglacials, as well as what drove it (Liu et al., 2014) – but the widespread permafrost thaw inferred here suggests that mean annual temperatures, and not simply those during summer, were higher during MIS 11 and 13 in high northern latitudes.

The Permafrost Carbon Feedback

If widespread permafrost thaw occurred during MIS 11 and 13, presumably the permafrost carbon feedback took effect. Curiously, atmospheric CO_2 and CH_4 concentrations were only at Holocene levels during MIS 11 and even lower during MIS 13 (Fig. 3e,f). Perhaps there was a smaller stock of stored carbon in the permafrost at the start of these interglacials relative to today. Indeed, a considerable fraction of permafrost soil carbon has accumulated over the Holocene (Walter-Anthony et al., 2014). Alternatively, the rate of permafrost carbon release may have been slow enough to be buffered by oceanic uptake, and thus not expressed in ice core records of atmospheric composition. This scenario may be supported by marine records of lysocline depth showing that MIS 11 featured the largest episode of carbonate dissolution during the past 500 kyr (Barker et al., 2006; Bauch et al., 2000; Helmke and Bauch, 2002). It is also possible that while additional carbon was released due to permafrost thaw, less carbon was released from other typical deglacial sources or more was taken up by increased plant and peat regrowth (Zech et al., 2012). In any case, permafrost thaw clearly did not yield atypical greenhouse gas concentrations during MIS 11 and 13, but the long time scales associated with permafrost carbon release and re-uptake may help to explain why concentrations remained at interglacial values longer than during the more sawtooth-shaped glacial cycles to follow (Fig. 3e,f) – perhaps contributing to the exceptional length of MIS 11.

The North American speleothem growth chronology presented here yields constraints on permafrost stability through previous episodes of warmth. Coupled with similar results from Siberia (Vaks et al., 2013), it suggests that there was widespread Arctic and sub-Arctic speleothem deposition, and thus ground thaw, extending into the continuous zone during the MIS 11 "super" interglacial (Melles et al., 2012), and, more puzzlingly, the MIS 13 "luke-warm" interglacial. These findings may have particular relevance to the future given that Arctic temperatures during these interglacials appear to have been comparable to those expected later this century. Carbon cycle modeling, together with integration of marine and ice core $\delta^{13}C$ records, might help to reconcile the unremarkable greenhouse gas changes observed across MIS 11 and 13 despite the potentially widespread thaw of Arctic permafrost then.

Methods

Speleothem Collection

Speleothems from the southern Canadian Rocky Mountains were collected by Derek Ford, Russ Harmon, P. Thompson, and Steve Worthington in 1968-1974 and 1984-1985. Samples from the Nahanni area were collected by Derek Ford, Russ Harmon, and George Brook in 1972-1973. Bernard Lauriol collected the northern Yukon speleothems between 1985-1995. Samples from Yukon-Charley Rivers National Preserve, Alaska were collected by Jeff Rasic in 2015 (National Park Service Accession YUCH-00253, catalog numbers 8385-8390).

U-Th Dating

$CaCO_3$ samples weighing between 0.02-1.98 g were drilled from speleothems using a dremel and/or dental drill with a 0.9 mm diameter drill bit. Powders were weighed, spiked with a mixed ^{229}Th-^{233}U-^{236}U tracer, and dissolved. Following the methods of Edwards et al. (1987), U and Th were removed from solution by co-precipitation with Fe oxyhydroxides, redissolved, and eluted separately through 0.5 mL bed volume columns packed with BioRad AG1-X8 resin. A total procedural blank was included in each set of chemistry (5-10 samples). U and Th measurements were made on a Nu Plasma II- ES MC-ICP-MS equipped with enhanced sensitivity to maximize resolution. Samples were introduced using a CETAC Aridus II desolvating nebulizer intake system. For a more detailed description, see Burns et al. (2016) and the supplementary information.

Null Probability Distribution

We calculated a hypothetical probability distribution of speleothem ages to compare to our observed distribution assuming uniform speleothem deposition per unit time during interglacials of the past 600 kyr (Fig. 3b), using beginning and ending ages of interglacials as defined by the LR04 $\delta^{18}O$ stack (http://www.lorraine-lisiecki.com/LR04_MISboundaries.txt). We modeled U-Th age uncertainties by fitting an exponential relationship to the observed North American Arctic speleothem data from this study, Harmon et al. (1977), and Lauriol et al. (1997): $1\sigma = 0.66*e^{0.0071*age}$. We also accounted for the decreased preservation of speleothems with age assuming that they have an effective half-life of 100 kyr (Scroxton et al., 2016). Although the actual half-life of speleothem survival in the Arctic may be higher or lower than this value, the general form of the resulting synthetic age distribution, with a relatively low probability of finding MIS 11 speleothems, is likely robust.

Acknowledgments

We thank Jeff Rasic and Yukon-Charley Rivers National Preserve for providing speleothems, Thomas Bauska, Ted Schuur, Peter Huybers for helpful discussion, and Caitlin Riggs for ArcGIS support. Research supported by NSF ARC-1607816 and 1607968.

References

Anthony, K. W., S. Zimov, G. Grosse, M. C. Jones, P. Anthony, F. S. Chapin III, J. Finlay, M. Mack, S. Davydov, and P. Frenzel (2014), A shift of thermokarst lakes from carbon sources to sinks during the Holocene epoch, Nature, 511(7510), 452-456.

Barker, S., D. Archer, L. Booth, H. Elderfield, J. Henderiks, and R. E. Rickaby (2006), Globally increased pelagic carbonate production during the Mid-Brunhes dissolution interval and the CO 2 paradox of MIS 11, Quaternary Science Reviews, 25(23), 3278-3293.

Bauch, H. A., H. Erlenkeuser, J. P. Helmke, and U. Struck (2000), A paleoclimatic evaluation of marine oxygen isotope stage 11 in the high-northern Atlantic (Nordic seas), Global Planet. Change, 24(1), 27-39.

Brown, J., O. Ferrians Jr, J. Heginbottom, and E. Melnikov (1997), Circum-Arctic map of permafrost and ground-ice conditions, US Geological Survey Reston, VA.

Burns, S. J., L. R. Godfrey, P. Faina, D. McGee, B. Hardt, L. Ranivoharimanana, and J. Randrianasy (2016), Rapid human-induced landscape transformation in Madagascar at the end of the first millennium of the Common Era, Quaternary Science Reviews, 134, 92-99.

Cheng, H., R. L. Edwards, C. Shen, V. J. Polyak, Y. Asmerom, J. Woodhead, J. Hellstrom, Y. Wang, X. Kong, and C. Spötl (2013), Improvements in 230 Th dating, 230 Th and 234 U half-life values, and U–Th isotopic measurements by multi-collector inductively coupled plasma mass spectrometry, Earth Planet. Sci. Lett., 371, 82-91.

Cronin, T. M., L. Polyak, D. Reed, E. S. Kandiano, R. Marzen, and E. Council (2013), A 600-ka Arctic sea-ice record from Mendeleev Ridge based on ostracodes, Quaternary Science Reviews, 79, 157-167.

de Vernal, A. and C. Hillaire-Marcel (2008), Natural variability of Greenland climate, vegetation, and ice volume during the past million years, Science, 320(5883), 1622-1625, doi:10.1126/science.1153929 [doi].

Dreybrodt, W. (1988), Processes in Karst Systems: Physics, Chemistry, and Geology, Springer, Berlin, 288.

Dreybrodt, W. (1999), Chemical kinetics, speleothem growth and climate, Boreas, 28(3), 347-356.

Edwards, R. L., J. Chen, and G. Wasserburg (1987), 238 U 234 U 230 Th 232 Th systematics and the precise measurement of time over the past 500,000 years, Earth Planet. Sci. Lett., 81(2), 175-192.

Fairchild, I. J. and A. Baker (2012), Appendix 1: Archiving speleothems and speleothem data, Speleothem Science: From Process to Past Environments, 368-370.

French, H. M. (1999), Past and present permafrost as an indicator of climate change, Polar Res., 18(2), 269-274.

Froese, D. G., J. A. Westgate, A. V. Reyes, R. J. Enkin, and S. J. Preece (2008), Ancient permafrost and a future, warmer Arctic, Science, 321(5896), 1648, doi:10.1126/science.1157525 [doi].

Harmon, R. S., D. C. Ford, and H. P. Schwarcz (1977), Interglacial chronology of the Rocky and Mackenzie Mountains based upon 230Th-234U dating of calcite speleothems, Canadian Journal of Earth Sciences, 14(11), 2543-2552.

Helmke, J. P. and H. A. Bauch (2002), Glacial–interglacial carbonate preservation records in the Nordic Seas, Global Planet. Change, 33(1), 15-28.

Koven, C. D., W. J. Riley, and A. Stern (2013), Analysis of permafrost thermal dynamics and response to climate change in the CMIP5 Earth System Models, J. Clim., 26(6), 1877-1900.

Lauriol, B., D. Ford, J. Cinq-Mars, and W. Morris (1997), The chronology of speleothem deposition in northern Yukon and its relationships to permafrost, Canadian Journal of Earth Sciences, 34(7), 902-911.

Lebron, I. and D. Suarez (1996), Calcite nucleation and precipitation kinetics as affected by dissolved organic matter at 25 C and pH> 7.5, Geochim. Cosmochim. Acta, 60(15), 2765-2776.

Lisiecki, L. E. and M. E. Raymo (2005), A Pliocene-Pleistocene stack of 57 globally distributed benthic $\delta^{18}O$ records, Paleoceanography, 20(1).

Liu, Z., J. Zhu, Y. Rosenthal, X. Zhang, B. L. Otto-Bliesner, A. Timmermann, R. S. Smith, G. Lohmann, W. Zheng, and O. Elison Timm (2014), The Holocene temperature conundrum, Proc. Natl. Acad. Sci. U. S. A., 111(34), E3501-5, doi:10.1073/pnas.1407229111 [doi].

Loulergue, L., A. Schilt, R. Spahni, V. Masson-Delmotte, T. Blunier, B. Lemieux, J. Barnola, D. Raynaud, T. F. Stocker, and J. Chappellaz (2008), Orbital and millennial-scale features of atmospheric CH4 over the past 800,000 years, Nature, 453(7193), 383-386.

Lüthi, D., M. Le Floch, B. Bereiter, T. Blunier, J. Barnola, U. Siegenthaler, D. Raynaud, J. Jouzel, H. Fischer, and K. Kawamura (2008), High-resolution carbon dioxide concentration record 650,000–800,000 years before present, Nature, 453(7193), 379-382.

Melles, M., J. Brigham-Grette, P. S. Minyuk, N. R. Nowaczyk, V. Wennrich, R. M. DeConto, P. M. Anderson, A. A. Andreev, A. Coletti, T. L. Cook, E. Haltia-Hovi, M. Kukkonen, A. V. Lozhkin, P. Rosen, P. Tarasov, H. Vogel, and B. Wagner (2012), 2.8 million years of Arctic climate change from Lake El'gygytgyn, NE Russia, Science, 337(6092), 315-320, doi:10.1126/science.1222135 [doi].

Past Interglacials Working Group of PAGES (2016), Interglacials of the last 800,000 years, Rev. Geophys., 54(1), 162-219, doi:10.1002/2015RG000482.

Raymo, M. E. and J. X. Mitrovica (2012), Collapse of polar ice sheets during the stage 11 interglacial, Nature, 483(7390), 453-456.

Reyes, A. V., A. E. Carlson, B. L. Beard, R. G. Hatfield, J. S. Stoner, K. Winsor, B. Welke, and D. J. Ullman (2014), South Greenland ice-sheet collapse during Marine Isotope Stage [thinsp] 11, Nature, 510(7506), 525-528.

Romanovsky, V. E., S. L. Smith, and H. H. Christiansen (2010), Permafrost thermal state in the polar Northern Hemisphere during the international polar year 2007–2009: a synthesis, Permafrost Periglacial Processes, 21(2), 106-116.

Schuur, E., A. McGuire, C. Schädel, G. Grosse, J. Harden, D. Hayes, G. Hugelius, C. Koven, P. Kuhry, and D. Lawrence (2015), Climate change and the permafrost carbon feedback, Nature, 520(7546), 171-179.

Scroxton, N., M. K. Gagan, G. B. Dunbar, L. K. Ayliffe, W. S. Hantoro, C. Shen, J. C. Hellstrom, J. Zhao, H. Cheng, and R. L. Edwards (2016), Natural attrition and growth frequency variations of stalagmites in southwest Sulawesi over the past 530,000 years, Palaeogeogr. , Palaeoclimatol. , Palaeoecol., 441, 823-833.

Slater, A. G. and D. M. Lawrence (2013), Diagnosing present and future permafrost from climate models, J. Clim., 26(15), 5608-5623.

Snyder, C. W. (2016), Evolution of global temperature over the past two million years, Nature, 538(7624), 226-228, doi:10.1038/nature19798 [doi].

Tarnocai, C., J. Canadell, E. Schuur, P. Kuhry, G. Mazhitova, and S. Zimov (2009), Soil organic carbon pools in the northern circumpolar permafrost region, Global Biogeochem. Cycles, 23(2).

Vaks, A., O. S. Gutareva, S. F. Breitenbach, E. Avirmed, A. J. Mason, A. L. Thomas, A. V. Osinzev, A. M. Kononov, and G. M. Henderson (2013), Speleothems reveal 500,000-year history of Siberian permafrost, Science, 340(6129), 183-186, doi:10.1126/science.1228729 [doi].

Willerslev, E., E. Cappellini, W. Boomsma, R. Nielsen, M. B. Hebsgaard, T. B. Brand, M. Hofreiter, M. Bunce, H. N. Poinar, D. Dahl-Jensen, S. Johnsen, J. P. Steffensen, O. Bennike, J. L. Schwenninger, R. Nathan, S. Armitage, C. J. de Hoog, V. Alfimov, M. Christl, J. Beer, R. Muscheler, J. Barker, M. Sharp, K. E. Penkman, J. Haile, P. Taberlet, M. T. Gilbert, A. Casoli, E. Campani, and M. J. Collins (2007), Ancient biomolecules from deep ice cores reveal a forested southern Greenland, Science, 317(5834), 111-114, doi:317/5834/111 [pii].

Zech, R. (2012), A permafrost glacial hypothesis–Permafrost carbon might help explaining the Pleistocene ice ages, Eiszeitalter und Gegenwart E&G/Quaternary science journal, 61(1), 84-92.Barker, S., D. Archer, L. Booth, H. Elderfield, J. Henderiks, and R. E. Rickaby (2006), Globally increased pelagic carbonate production during the Mid-Brunhes dissolution interval and the CO 2 paradox of MIS 11, Quaternary Science Reviews, 25(23), 3278-3293.

Figures

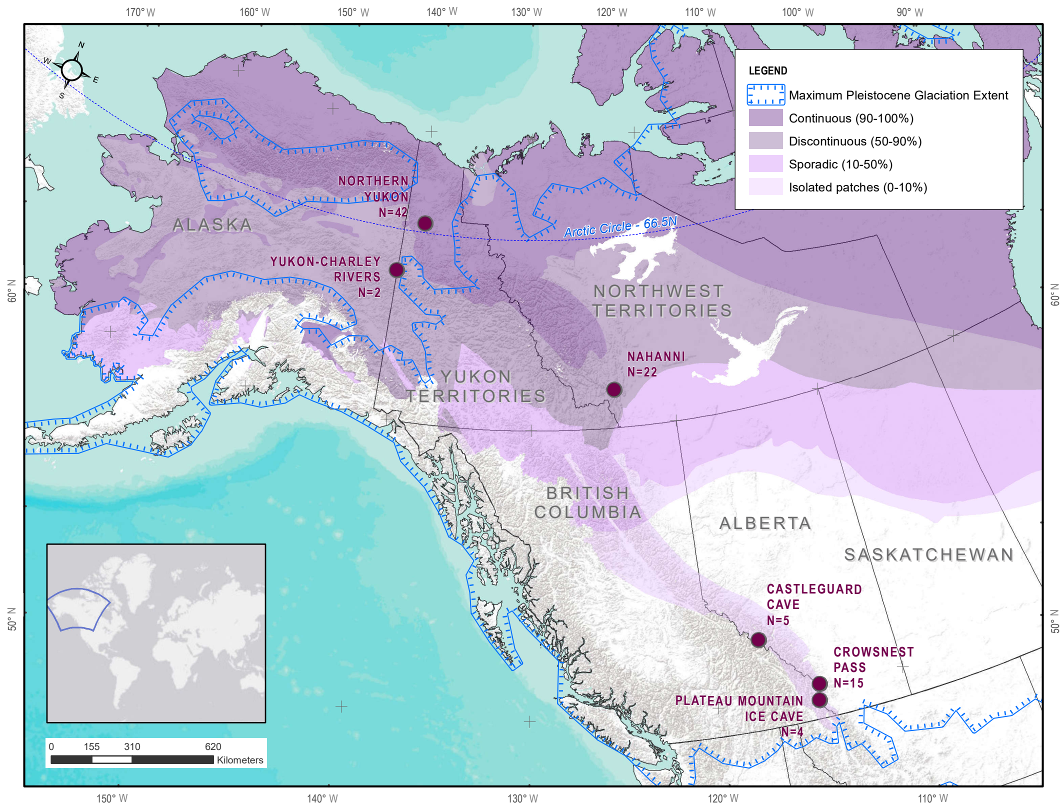

Figure 1: Current permafrost extent and sampled caves. Current permafrost zones in North America (Brown et al., 1997) (purple shading), maximum Pleistocene glaciation extent (blue hatched line), and locations of caves where speleothems were collected with the number of U-Th ages measured.

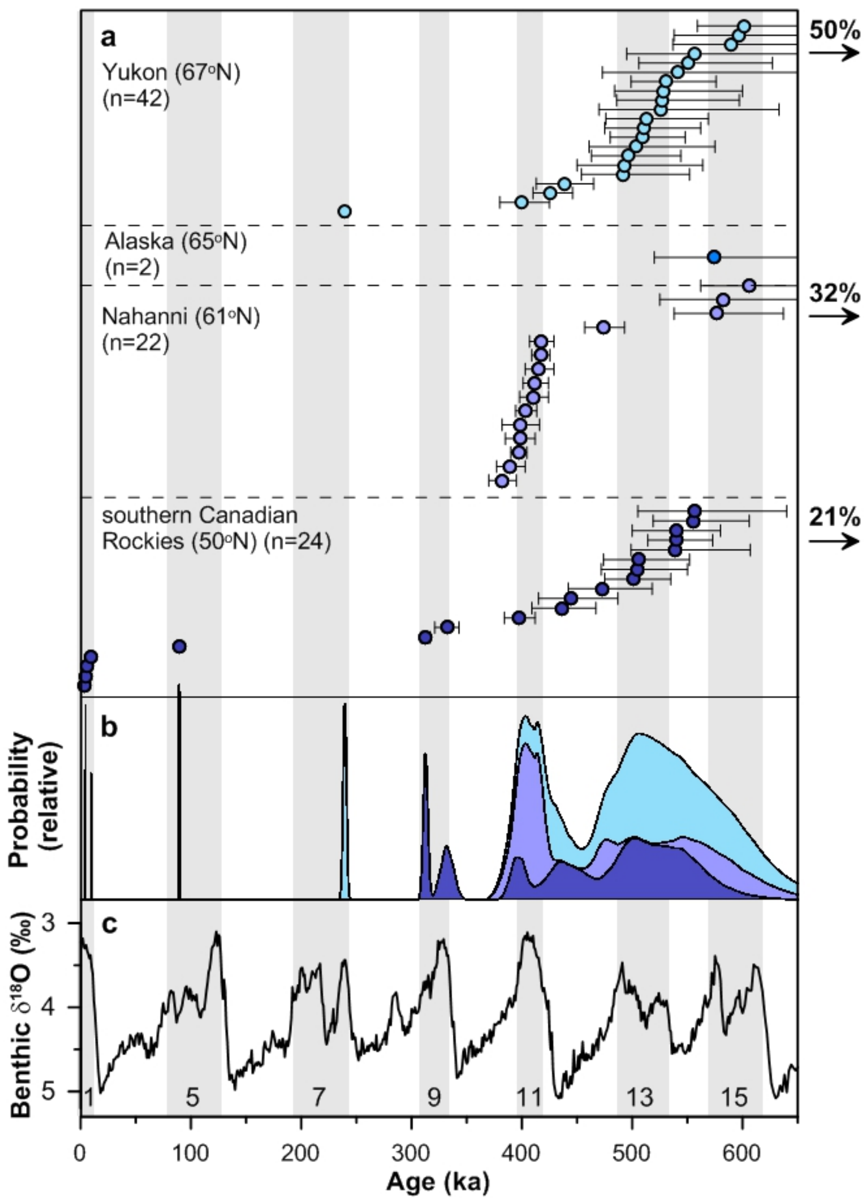

Figure 2: North American speleothem ages. **(a)** U-Th ages with 2σ uncertainties from the study regions, arranged by latitude. N values give the number of samples dated in each region, and percentages to the right show the proportion of samples dating beyond the U-Th limit. **(b)** Probability distributions of the U-Th ages, color-coded by regions shown in panel a (the single finite age from Alaska is not shown). **(c)** LR04 benthic $\delta^{18}O$ stack (Lisiecki and Raymo, 2005). Interglacial stages are numbered at bottom.

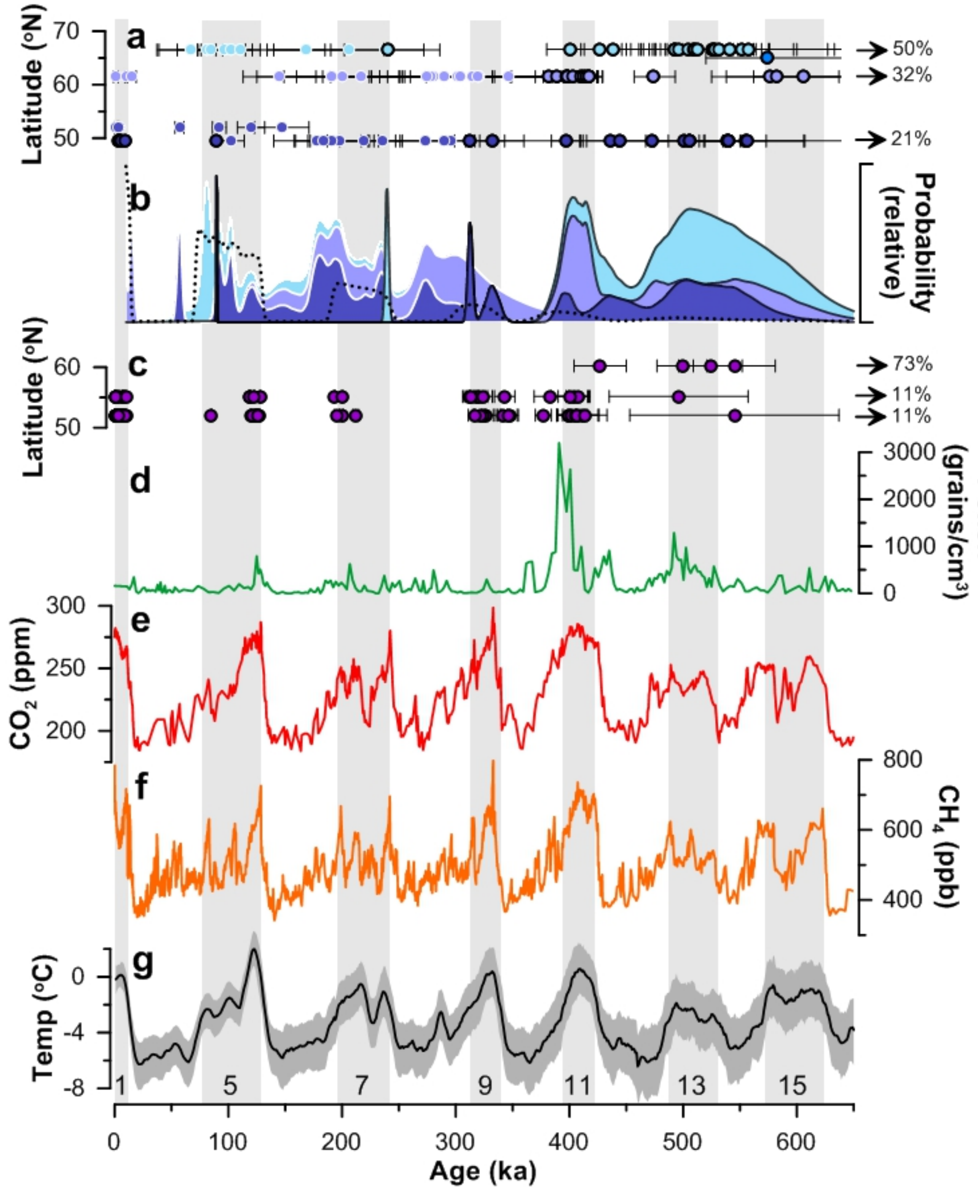

Figure 3: Arctic speleothem growth and paleoclimate records. (a) North American speleothem ages obtained in this study with ICP-MS (black borders), and from earlier alpha-spectrometry dating in the same caves (Harmon et al., 1977; Lauriol et al., 1997) (white borders), with 2σ uncertainties. Note that ages <350 ka in the northernmost region (lightest blue) are exclusively from speleothems at seasonally-warm cave entrances, and thus do not suggest substantial permafrost thaw (Lauriol et al., 1997). Percentages on right give proportion of ages obtained in this study beyond the U-Th limit. **(b)** Probability distributions of speleothem ages shown in panel a (same color scheme). The dotted black line shows a null probability distribution function assuming that speleothem deposition occurred evenly throughout interglacials but that speleothem preservation decreases with time (see Methods). **(c)** Siberian speleothem ages with 2σ

uncertainties (Vaks et al., 2013). Percentages on right give proportion of ages beyond the U-Th limit. **(d)** Pollen concentrations in a marine sediment core off southern Greenland (deVernal and Hillaire-Marcel, 2008). **(e)** Atmospheric CO_2 concentrations (Luthi et al., 2008). **(f)** Atmospheric CH_4 concentrations (Loulergue et al., 2008). **(g)** Global temperature (Snyder, 2016). Interglacial stages are numbered at bottom.

Tables

Table 1: Statistics of caves sampled in this study.

Region	Permafrost Zone	MAT (°C) [a]	Cave	Lat (DD)[b]	Lon (DD)	Elev (m asl)	Aspect	Cave Length (m)	Number of Speleothems Dated	MIS 11 Speleothem Growth in Cave Interior	MIS 13 Speleothem Growth in Cave Interior
northern Yukon	Continuous	-8	Bear Cave	66.5	139.3	867		220	14	X	X
northern Yukon	Continuous	-8	Tsi-tche-Han Cave	66.8	139.3	750		40	2		
northern Yukon	Continuous	-8	Grotte de la Chèvre	66.7	139.3	900			3		X
northern Yukon	Continuous	-8	Caverne des Méandres	66.8	139.3	900		100	3		X
northern Yukon	Continuous	-8	Grande Caverne Glacée	66.7	139.3	900		90	3		
northern Yukon	Continuous	-8	Grotte Disparue	66.7	139.3	900-1100		Cave remnant	4		
Yukon-Charley Rivers	Discontinuous		Funnel Creek Pass Cave	65.1	141.0	250		26	2		
Nahanni	Discontinuous	-5 to -7	Grotte Valerie	61.3	124.1	700		1000	4	X	
Nahanni	Discontinuous	-5 to -7	Igloo Cave	61.3	124.1	900		200	1		
Nahanni	Discontinuous	-5 to -7	Ice Curtain Cave	61.3	124.1			100	1		
Nahanni	Discontinuous	-5 to -7	Speleothem Cave	61.3	124.1			30.5	4	X	X
Nahanni	Discontinuous	-5 to -7	Fault Cave	61.3	124.1				1	X	
southern Canadian Rockies	Isolated		Castleguard Cave	52.1	117.3	1970-2445		21000	5	X	
southern Canadian Rockies	Isolated		Plateau Mountain Ice Cave	50.16	114.5		S	>400	4		X

southern Canadian Rockies	Isolated	Coulthard Cave	49.5	114.5	2440	N	370	1		X
southern Canadian Rockies	Isolated	Middle Sentry Cave	49.5	114.5	1860		75	1		X
southern Canadian Rockies	Isolated	Yorkshire Pot	49.5	114.5	2410		13800	1		
southern Canadian Rockies	Isolated	Boon’s Glittering Ice Palace	49.5	114.5	2226		286	1		
southern Canadian Rockies	Isolated	Gargantua Cave	49.5	114.5	2501		5940	6	X	X
southern Canadian Rockies	Isolated	Eagle’s Nest Cave	49.5	114.5	1377		60	1		X

[a]MAT = Mean Annual Temperature
[b]DD = Decimal Degrees

Supplementary Material

Cave Descriptions and Speleothems

Northern Yukon

Bear Cave Mountain (990 m) and the Tsi-it-toh-Choh Range (1219 m) are in the northern Ogilvie Mountains on the Arctic Circle, an area that was never covered by Quaternary glaciers (Hughes, 1972; Zazula et al., 2004). Numerous horizontally oriented caves lie on the sides of the mountains at 700-1000 m, a few hundred meters above the Fishing Branch River, which runs from 500-450 m (Lauriol et al., 1997). The caves are mainly developed in Devonian limestone beds of the Gossage and Ogilvie formations that were deformed at the end of the Cretaceous to the start of the Tertiary (Norris, 1978; Lauriol et al., 2001). The current regional climate is cold continental and the area lies north of the continuous permafrost boundary. Mean annual air temperature (1981-2010) at the Old Crow meteorological station, 125 km to the northwest and at 220 m elevation, is -8˚C, and there are 278 mm of yearly precipitation, half falling as snow (Environment Canada, 2017). Many of the caves contain ice that likely results from topoclimatic zonation: Zone 1 is near entrances with temperatures above freezing and humidity around 80%, some of this water vapor freezes as ice deeper in the cave (Zone 2) where humidity approaches 100% and air temperatures are below freezing near the ground and above freezing near the ceiling, and Zone 3 is cold and dry with air temperatures around -2˚C and humidity 60-65% (Lauriol et al., 1988, 2016). Currently, the presence of permafrost does not allow seepage water through fissures in the rock to reach the caves, and thus active speleothem deposition has not been observed (Lauriol et al., 1988). Lauriol et al. (1997) U-Th dated 24 speleothems from Bear Cave and Tsi-tché-han Cave where the only speleothems to return finite ages were collected at cave entrances (dating to MIS 5 and 7); samples collected from cave interiors were infinite, which they interpreted to suggest minor interglacial thickening of the active layer but otherwise persistent permafrost conditions throughout the Quaternary.

Bear Cave is located at 66˚30' N, 139˚20' W and 867 m elevation in Bear Cave Mountain, about 400 m above the valley floor. It is nearly horizontal, 220 m in length, and consists of three main chambers and a few smaller passages (Lauriol et al., 1997). The second chamber contains clear pillars of ice and small hoar crystals coat the ceilings and walls. The third chamber is dry with a few very large hoar crystals and contains numerous speleothems including flowstones and thick bosses (3-4 m thick) (Lauriol et al. 1997). Some speleothems are deposited on silts or gravels that are indicative of preceding fluvial phases of infilling and partial re-excavation. The third chamber was accessible from the second chamber in 1987, but this entry point was blocked by ice in 1997 and it was accessed from the first chamber instead (Lauriol, 2016). Snow tends to block the cave entrances in the winter (Lauriol, 2016). Air temperatures in the rear of the cave (Zone 3) were between -1 to -3.8˚C in July 1985 and 1987 (Lauriol et al., 1988).

Tsi-tché-han Cave is located at 66˚49' N, 139˚20' W and 750 m elevation in the Tsi-it-toh-Choh Range. It is 40 m in length with two interior chambers. Two passages lead off from the outer entrance chamber (18 m long, 6 m wide, and 2-3 m high): a short passage obstructed by ice, and a longer passage (10 m long and 1 m wide) ending in a second inner chamber (10 m long, 6 m wide, 2 m high) that was blocked by ice in 1997 but appears to lead to other openings. The walls of the second chamber are well decorated with flowstone (Lauriol et al., 2001). Measured ground temperature in July 1985 was 4˚C halfway into the first chamber, 1.4˚C at the back of the first chamber, and 0˚C five meters beyond (Lauriol et al., 1988). Air temperatures in the rear of the cave (Zone 3) were between -1 to -3.8˚C in July 1985 and 1987 (Lauriol et al., 1988).

Caverne des Meandres is located at 66˚46'N, 139˚17'W, and is 100 m long, 2-3 m wide and 2-4 m high (Lauriol et al., 2006). An ice plug 30 m from cave entrance blocks the end of a passage and contains broken calcite concretions (Lauriol et al., 2001).

Grotte Disparue is located at 66˚42'N, 139˚15'W at an altitude of 900-1100 m. It is a remnant of a former solution cave on a slope of Tsi-it-toh-Choh Mountain.

Grande Caverne Glacée is located at 66˚42'N, 139˚18'W, 900 m asl and measures 90 m in length, 5-8 m wide, and 3 m in height (Lauriol et al., 1997). It contains well-preserved organic remains with a spruce wood fragment embedded in massive ice dating to 7350 years BP. Temperatures in late June 1992 were above freezing along the cave ceiling but decreased to 0˚C at the back of the cave, and ranged from -1.5 to 0˚C along the floor (Lauriol et al., 2006).

Caverne '85 is located at 66˚46'N, 139˚17', 900 m asl. It is 40 m long, 1-2 m wide, and reaches almost 4 m in height (Lauriol et al., 2006). Hoar frost covers the walls beyond 30 m from the entrance and thickens with depth in the cave (Lauriol et al., 1988). The back of the cave is blocked by a 4 m wide, 2.5 m tall wall of ice (Lauriol et al., 1988).

Grotte de le Chevre is located at 66˚41'N, 139˚16', 900 m asl.

Yukon-Charley Rivers National Preserve, Alaska

Yukon-Charley Rives National Preserve is located along the Canadian border in discontinuous permafrost of east-central Alaska (Daum, 1994) where elevations range from 150 to 1950 m (Allen et al., 2008). Funnel Creek is a tributary to the Tatonduk River before its confluence with the Yukon River situated in steep, rugged, limestone mountains. Modern vegetation largely includes boreal forest highly fragmented by large limestone outcrops, taluses, and open steppe-like slopes with alpine tundra at elevation (Parker et al., 1995). This area was not glaciated during the Pleistocene.

Funnel Creek Pass Cave is located at 65˚4'40.98"N, 141˚2'42.32"W and about 250 m above a valley floor and 30 m below the top of a ridge. The cave entrance is 4 m wide and 3.1 m high. The initial chamber extends 11 m toward the north and decreases to 1.5 m in height at the back. A second chamber extends 15 m further after a sharp turn to the southwest. The second chamber slopes upward at about 20˚ and narrows (Jeff Rasic, Yukon-Charley Rivers National Preserve archaeologist, personal communication, 2015).

Nahanni Plateau, Northwest Territories

This region is located in the Mackenzie Mountains at 61˚N, 124˚W (Harmon et al, 1977) and in the discontinuous permafrost zone. It has a cold continental climate with mean annual temperatures of -5 to -7˚C and annual precipitation of ~550 mm (Ford, 1993). The South Nahanni River passes through three antecedent canyons (over 100 km) composed of limestones, dolomites and calcareous shales (Ford 1976, 2011). The significant karst rock is limited to the Nahanni Formation (Middle Devonian), massively bedded and very pure limestone 180 m in thickness that forms the rim of the First (furthest downstream) Canyon (Ford, 2009). There are more than 100 apparent cave mouths in the limestone walls of the First Canyon and Lafferty Canyon (Ford, 1973). Many of the studied caves are relict fragments of much larger phreatic caves that have been retreating through time (Ford, 1973). Summer temperatures near cave entrances can seasonally reach above 0˚C and consequently there is limited calcite deposition at and close to south-facing cave entrances (Ford, 1973; Brook, 1976). Cave interiors, however, maintain sub-freezing temperatures year round and there is no deposition (Brook, 1976). Harmon et al. (1977) dated 27 samples from 17 speleothems in several caves from this region with alpha spectrometry, with 19 returning finite ages. Uncertainties are large, but these ages generally seem to be associated with interglacials.

Grotte Valerie is one of the most extensive cave systems in the area, with more than 1000 m of mapped passages. It is located 450 m above the South Nahanni River in the north wall of the First Canyon at 61˚17' N, 124˚5' W and 700 m elevation (Ford, 1973). It is a relict stream cave and its entrance has retreated considerably due to cliff recession. The external mean annual temperature of the plateau 50 m above the cave is estimated to be -7˚C, and it is largely permafrozen (Ice Caves in Canada, In Press). Temperature studies here suggest distinct zonation in the cave, which enable different features to develop; Zone 1 includes the warmer cave entrances (+6 to +1˚C, measured in 1971) where active deposition of small calcite stalactites and flowstones indicates that the rock above is partially to fully thawed; Zone 2 (0 to -1.5˚C in 1971) contains ice sheets, ice stalactites, and hoarfrost crystals due to water vapor infiltrating from Zone 1 and freezing; in Zone 3, the passages descend below the levels of cave entrances, which enables very cold and dense winter air to remain throughout summer (-3˚C in summer of 1972), and water is unable to penetrate the frozen rock cover (Brook, 1976).

Igloo Cave is found in the south wall of Death Canyon at approximately 61˚17' N, 124˚7' W and 900 m asl in the vicinity of Speleothem Cave, and is a relict fragment of a large phreatic cave. It is ~200 m in total length and includes one large room. Most of the chambers and passages are below the level of the cave entrance and thus function as a cold trap that has accumulated dripstone ice (-4˚C in summer of 1973) (Brook, 1976).

Ice Curtain Cave is located in the north wall of Death Canyon at approximately 61˚17' N, 124˚7' W. It is 100 m long, with a 17 m tall and 7 m wide entrance. Similar temperature zonation to that found in Grotte Valerie also occurs here, with a warmer entrance and actively growing helicticites, a mixed temperature second zone with ice formations, and a permafrozen third zone.

Speleothem Cave is a relict fragment located in the north wall of a karst corridor known as Stal Gorge, near 61˚17' N, 124˚7' W, 40 km north of First Canyon. The cave is 30.5 m long and was formed by solution under phreatic groundwater flow conditions. It contains evidence of speleothem deposition followed by episodic stream flow, which eroded many of the formations – broken speleothems are common here and mostly located in the cave entrance, which has retreated due to cliff recession.

Fault Cave is a short relict cave near Speleothem Cave (61˚17' N, 124˚7' W) that also contains numerous frost-shattered speleothems.

Southern Canadian Rockies, Alberta-British Columbia

Despite its southerly latitude this region is located in the isolated permafrost zone due to alpine conditions in the Front and Main ranges of the southern half of the Canadian Rocky Mountains. Caves are often found in the extensively glaciated high alpine karst.

Castleguard Cave is located at 52˚6’ N, 117˚15’ W (Gascoyne et al., 1983), and rises from 1970 to 2245 m asl in Castleguard Mountain. It is 21 km long and was formed by groundwater flowing NW-to-SE from sources under the central mass of the Columbia

Icefield. The cave is primarily developed in the Cathedral limestone formation and secondarily composed of the Stephen Formation and the lower Eldon Formation, all of Cambrian age. Most of the accessible areas of the cave are drained relicts, with water currently passing down through them to lower routes. Additional relict passages at the upper end of the cave, beneath ~200 m of glacier ice, terminate in sealed ice blockages that appear to be ablating slowly (Ford et al., 1976). Mean internal air temperature is 2.4˚C with minimal seasonality (Atkinson et al., 1983).

Plateau Mountain Ice Cave is located on Plateau Mountain at 50˚10' N, 114˚30' W in the Livingstone limestone formation (Mississippian) (Harris and Pedersen, 1998). The flat mountain top was not glaciated during the late Pleistocene and its summit permafrost is a relict from the Last Glacial Maximum that has not yet reached equilibrium with current climate (Harris and Brown, 1978; Ice Caves in Canada, In Press). The cave entrance lies in a south facing wall at 2,225 m elevation near the north end of Plateau Mountain, and it extends for >400 m into the permafrost at a shallow depth, with temperatures decreasing inwards (Harris, 1979).

Numerous caves are found in the Crowsnest Pass area at approximately 49.5˚N, 114.5˚W. The pass is a major east-west breach through successive cuestas of the Front Ranges in the southernmost Canadian Rockies. Trough valleys run through relict aquifers, leaving cave-containing remnants exposed (Ford, 1993; Harmon et al., 1977), including Coulthard Cave, Middle Sentry Cave, Yorkshire Pot, Boon's Glittering Ice Palace, and Gargantua Cave. These caves span 1400 to 2500 m asl and a wide range of conditions, from modern boreal forest at the lower sites to high alpine tundra where cave temperatures never exceed freezing. Most caves were covered by glaciers during the Last

Glacial maximum. They are deglaciated but entrances are filled by snow during winter (Rollins, 2004). All of the caves are well ventilated today, and growing only a few small speleothems, if any. The samples we measured were all from inactive, broken, usually frost-shattered deposits.

Coulthard Cave is located at 2440 m asl on the north face of Mt. Coulthard. The lone entrance is 7 m wide, and the cave is 370 m long and up to 61 m deep (Rollins, 2004). All but one of the cave passages end in nearly vertical ice blockages. Cave temperatures remain below freezing year round (Marshall and Brown, 1974).

Middle Sentry Cave is situated at 1860 m asl. It is 75 m long and 10 m deep, and has two entrances (Rollins, 2004).

Yorkshire Pot is a complex multi-level cave with relict phreatic and underlying active stream passages. It is 13.8 km in length, 390 m in depth, highest entrances at 2410 m asl. Samples are from relict passages with weakly positive temperatures today; some small but active speleothems are also growing in them.

Boon's Glittering Ice Palace lies at 2226 m asl, it is 286 m long, and spans 84 m vertically. It has numerous skylights and is composed of three passages. As its name suggests, there are several ice slopes as well as an ice-decorated room at the end of the Gothic Passage (Rollins, 2004).

Gargantua Cave is entered at 2501 m asl and has 5940 m of passages that descend 286 m. Its upper chamber is the largest cavern in Canada at 290 m long, 30 m wide, and 25 m tall (Rollins, 2004); it has a negative mean temperature. Lower passages have weakly positive temperatures and some modern speleothem growth.

Eagle's Nest Cave is located at 1377 m asl and is approximately 60 m in length (Harington, 2011; Rollins, 2004). It is a relict outlet passage located approximately 90 m above the active Crowsnest Spring Cave.

U-Th Dating

U-Th samples were processed at MIT in a clean laboratory equipped with HEPA-filtered air and ULPA-filtered laminar flow hoods. The U-Th isotope tracer was prepared by mixing a ^{229}Th solution with the 3636a ^{233}U-^{236}U solution from the Institute for Reference Materials and Measurements. It was calibrated by mixing with U-Th gravimetric standards prepared from solid uranium (CRM 112a) and thorium (Ames Th bar) metals at MIT, followed by measurements of $^{238}U/^{236}U$ and $^{232}Th/^{229}Th$ in the combined solution. The tracer U-Th ratio was validated by measurements of the GC-1 secular equilibrium standard and the University of Minnesota aliquot of HU-1 (Cheng et al., 2013). Tracer validation samples were prepared and analyzed using the same methods as used for samples in this study.

For most samples, uranium isotopes were measured in a static analysis with ^{238}U, ^{236}U, ^{235}U and ^{233}U measured on Faraday cups and ^{234}U measured on a secondary electron multiplier (SEM). The Faraday cup measuring ^{233}U was equipped with a 10^{12} ohm resistor, while the other cups had a 10^{11} ohm resistor. Samples were bracketed by measurements of unspiked CRM 112a measured with the same detectors. Measurements at masses 237, 236.5, 234.5 and 233.5 on the SEM were performed using a dynamic routine after each on-mass measurement. Signals at 237 and 236.5 were used to fit a power law to the tail from ^{238}U; this relationship was then applied to estimate the down-mass tails from ^{236}U and ^{235}U and to remove the effects of tailing on all masses except

^{238}U. Tailing at ^{234}U was consistently 2-4 per mille of the total ^{234}U intensity. Once per day, upmass tailing and hydride formation were measured by measurement at masses 238.5, 239 and 239.5. The combined upmass tail and hydride was consistently 1-2 x 10^{-6} relative to the ^{238}U beam. This signal was multiplied by the ^{233}U intensity and removed from the ^{234}U beam for each sample. Ion counter yield was determined using $^{234}U/^{238}U$ ratios measured in bracketing CRM 112a standard measurements after correction for tailing as described above and correction for mass bias using measured $^{238}U/^{235}U$ ratios in bracketing standards. Backgrounds for both on-mass and tailing measurements were determined by measurements of blank acid using the same detector array prior to each analysis.

Thorium isotope analyses were performed in static mode with ^{232}Th measured in a Faraday cup with a 10^{11} ohm resistor, ^{230}Th measured in an SEM, and ^{229}Th measured in a Faraday cup with a 10^{12} ohm resistor. Measurements were bracketed by measurements of an internal ^{232}Th-^{230}Th-^{229}Th standard (MITh-1) calibrated by measurement of an admixed ^{233}U-^{236}U solution (IRMM 3636a). Standard analyses were used to determine mass bias and ion counter yield. Tailing from ^{232}Th on ^{230}Th was measured once per day using dynamic measurement of masses 230.5 and 229.5 on the SEM; as tailing from ^{232}Th on ^{230}Th was consistently <0.3 ppm and we excluded samples with $^{230}Th/^{232}Th$ ratios <100 ppm, variations in this tailing comprised a minor portion of uncertainty for our samples.

For a small number of samples, all isotopes of U and Th fractions were measured using Faraday cups in a static analysis to reduce uncertainties associated with ion counter yield variability. For uranium, ^{238}U was collected in a Faraday cup equipped with a 10^{10}

ohm resistor, and ^{234}U was collected in a Faraday cup equipped with a 10^{12} ohm resistor. All other cups had 10^{11} ohm resistors. For thorium, ^{230}Th was measured in a cup with a 10^{12} ohm resistor. Uranium and thorium analyses were bracketed by the same standards as above but with higher concentrations. Tailing of higher masses on ^{234}U was estimated from $^{234}U/^{238}U$ ratios in bracketing standards after correction for mass bias.

Uncertainties reported for isotope ratios incorporate uncertainties associated with background, tailing, mass bias, ion counter yield variability, spike composition, and procedural blanks. U-Th ages were calculated using the ^{238}U decay constant of Jaffey (1971) and the ^{234}U and ^{230}Th decay constants of Cheng et al. (2013). U-Th ages were corrected for initial ^{230}Th assuming an initial $^{230}Th/^{232}Th$ ratio of 4.4 (± 2.2) x 10^{-6} (atomic); samples with $^{230}Th/^{232}Th$ <80 ppm were excluded. U-Th age uncertainties incorporate analytical, initial ^{230}Th and decay constant uncertainties and were calculated with a Monte Carlo routine using MATLAB software. All U-Th data are given in Supplementary Table 1.

Supplementary Figures

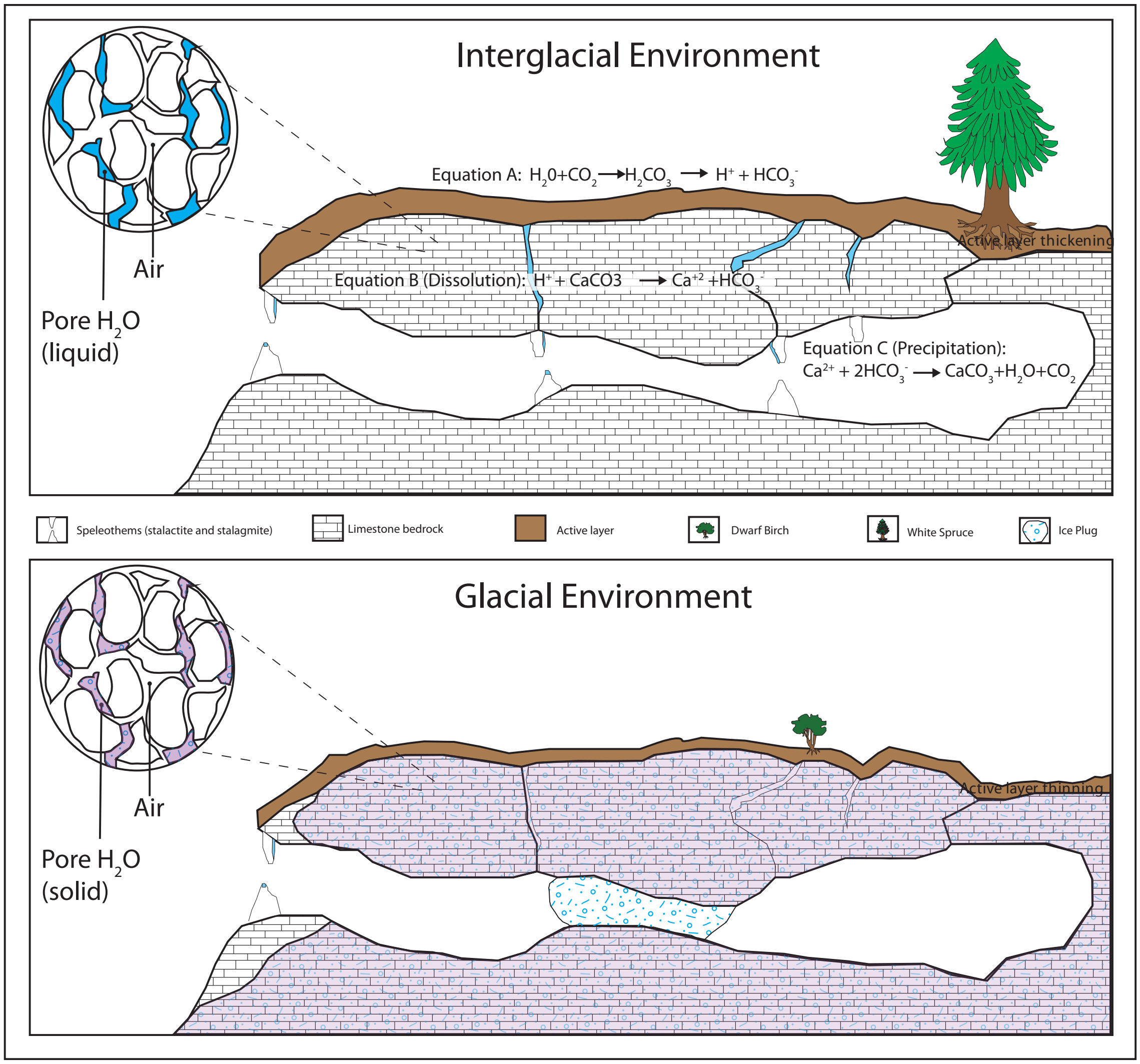

Supplementary Figure S1: A conceptual diagram of Arctic speleothem growth. (Top) Interglacial conditions are more suitable for speleothem deposition, since water can percolate downward into the cave. (Bottom) When permafrost is abundant, deposition ceases due to blockage of seepage water by perennially frozen ground, reduced biogenic CO_2 input due to sparse vegetation, reduced cave ventilation associated with snow/ice plugs in the cave or at cave entrances, and reduced temperatures.

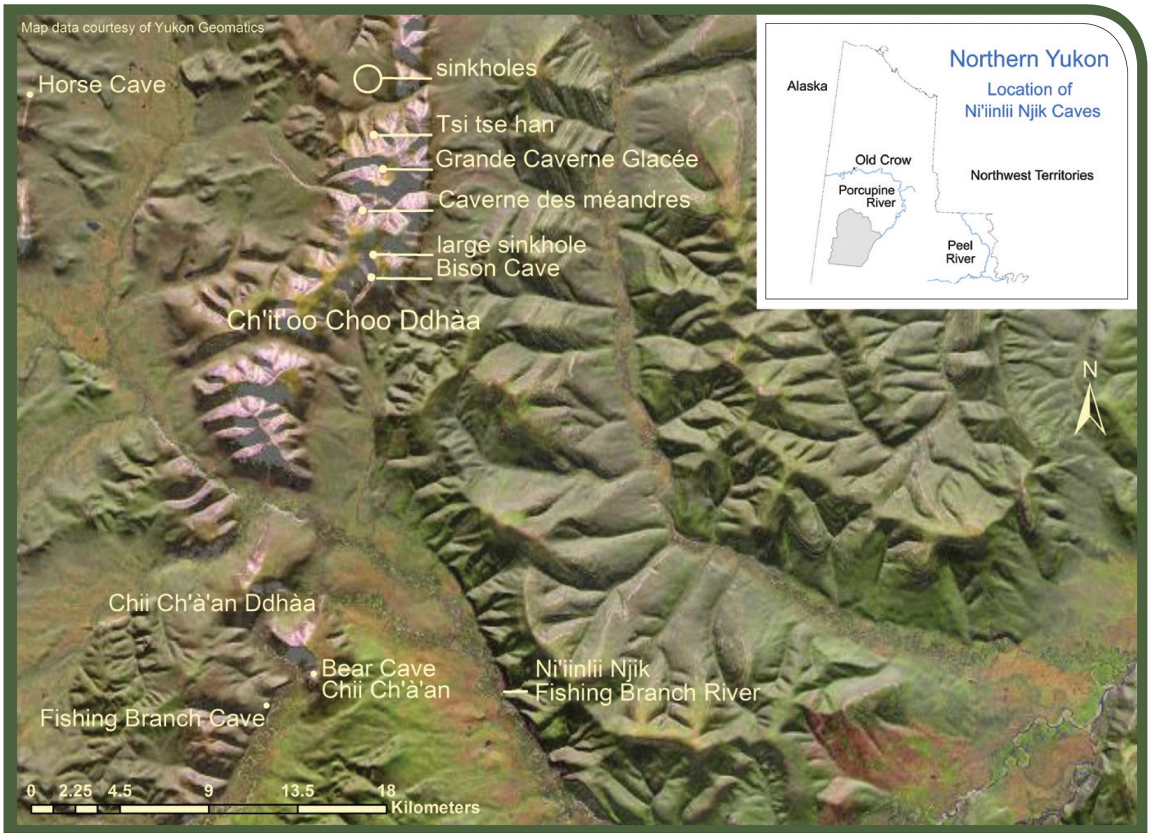

Supplementary Figure S2: Shaded relief map of the northern Ogilvie Mountains showing locations of the northern Yukon caves (from Lauriol, 2016).

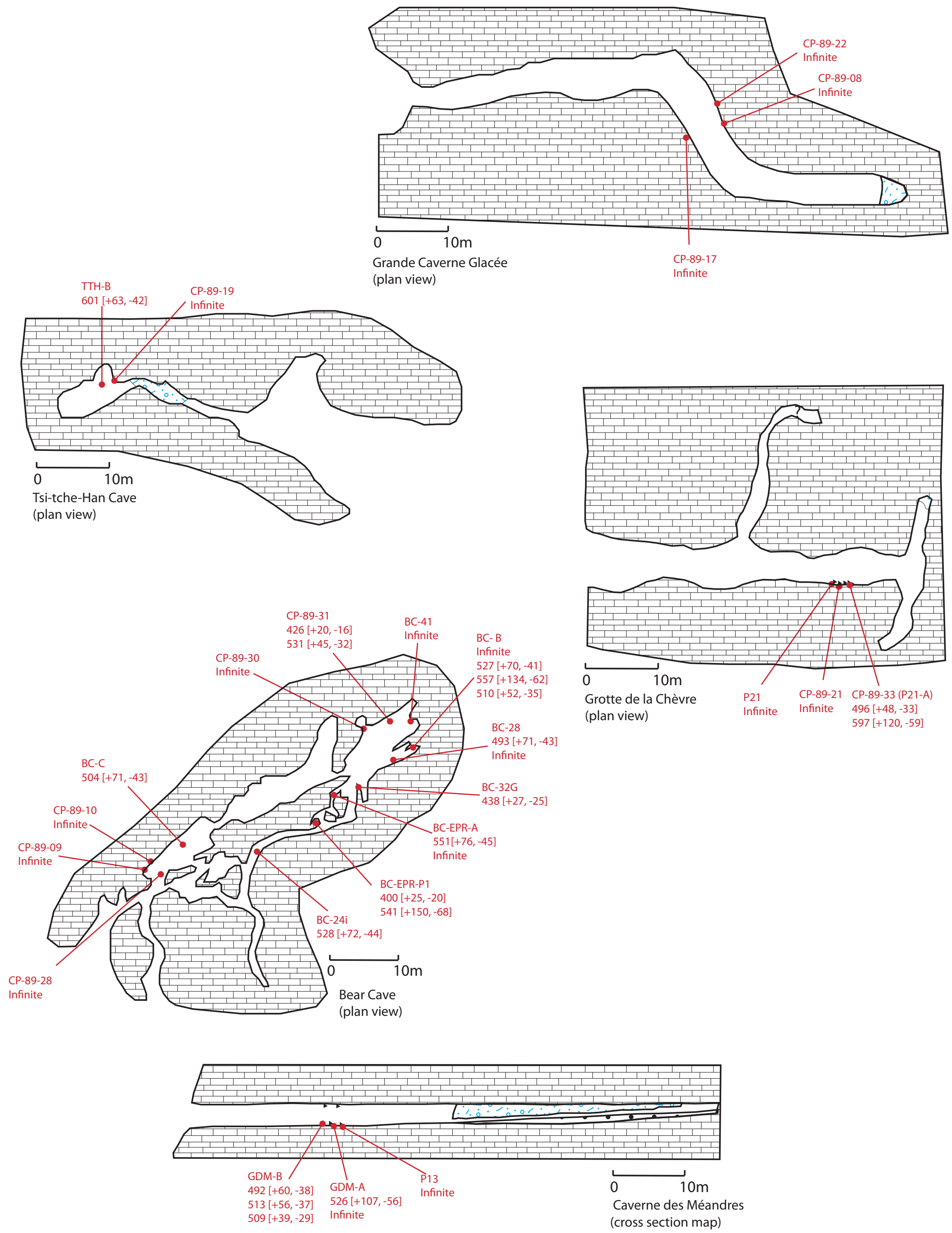

Supplementary Figure S3: Maps of northern Yukon caves with locations and U-Th ages of speleothem with 2σ uncertainties (in kyr).

Supplementary Figure S4: Speleothems from the northern Yukon Caves, showing U-Th sample locations (dashed red) and ages with 2σ uncertainties (in kyr).

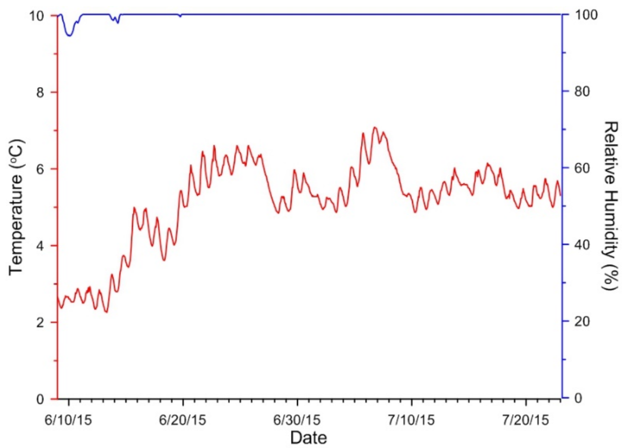

Supplementary Figure S5: Temperature (red) and relative humidity (blue) measured in the back of Funnel Creek Pass Cave during summer 2015 (Data from Jeff Rasic, Yukon-Charley Rivers National Preserve archaeologist).

Supplementary Figure S6: The entrance of Funnel Creek Pass Cave (Image from Jeff Rasic, Yukon-Charley Rivers National Preserve archaeologist).

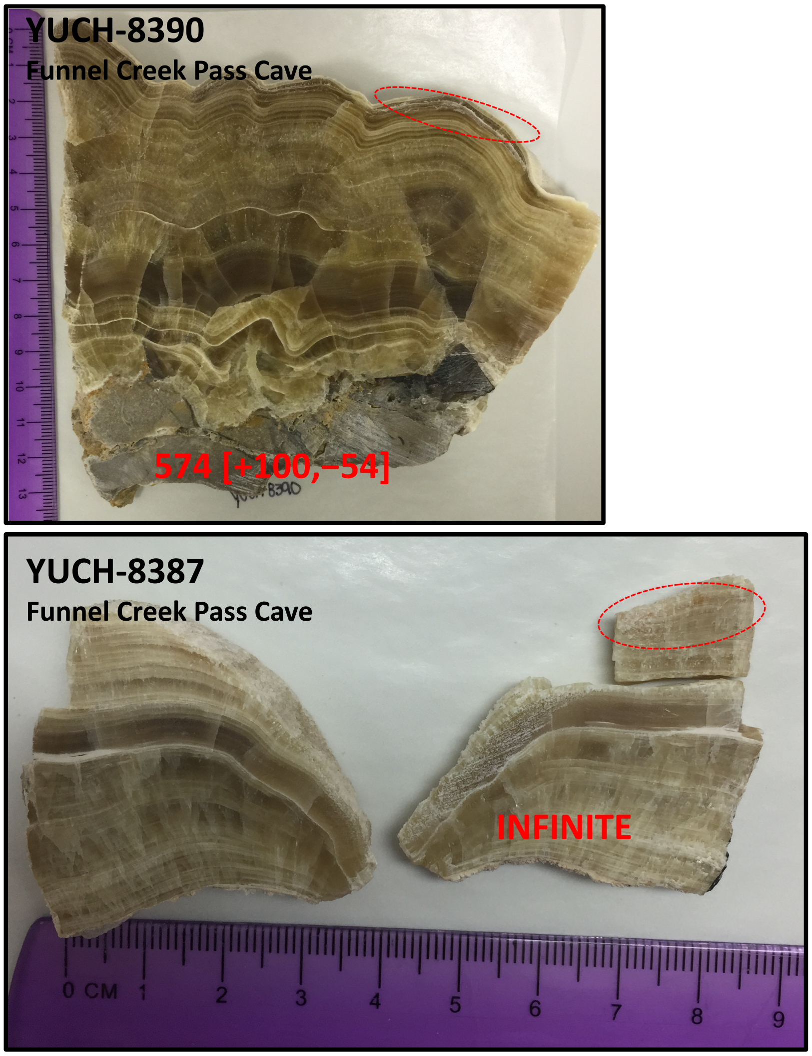

Supplementary Figure S7: Flowstones from Funnel Creek Pass Cave, showing U-Th sample locations (dashed red) and ages with 2σ uncertainties (in kyr).

Supplementary Figure S8: Speleothems from the Nahanni Plateau, showing U-Th sample locations (dashed red) and ages with 2σ uncertainties (in kyr).

Supplementary Figure S9: Speleothems from the southern Canadian Rockies, showing U-Th sample locations (dashed red) and ages with 2σ uncertainties (in kyr).

Supplementary Tables

Supplemental Table S1: North American speleothem U-Th ages used in Fig. 2 and 3

Region	Sample ID	^{238}U (ng/g)[a]	± (2σ)	^{232}Th (pg/g)[a]	± (2σ)	^{232}Th (pg/g)[a]	± (2σ)	($^{230}Th/^{238}U$) activity	± (2σ)	$^{230}Th/^{232}U$ ppm atomic	± (2σ)	Age (ka) (uncorrected)[c]	Unc - (2σ)	Unc + (2σ)	Age (ka) (corrected)[d]	Unc – (2σ)	Unc + (2σ)	$\delta^{234}U$ initial (per mil)[e]	± (2σ)
Yukon-Charley, Alaska	YUCH 8390	1173	23	213	4	0.1	0.5	0.9948	0.0024	86790	249	574	53	100	574	54	100	7	6
Yukon-Charley, Alaska	YUCH 8387	473	9	107	2	12.2	0.4	1.0397	0.0048	73276	512				>600				
southern Canadian Rockies	73045	1428	29	7609	153	396.0	2.2	0.0476	0.0010	142	3	3.78	0.08	0.08	3.66	0.09	0.09	400.0	2.0
southern Canadian Rockies	87013	1290	26	776	17	1072.8	1.4	0.0830	0.0010	2188	31	4.44	0.05	0.05	4.43	0.06	0.06	1086.0	1.0
southern Canadian Rockies	87013-10	1690	30	392	14	1082.1	0.8	0.1127	0.0005	7700	200	6.04	0.03	0.03	6.04	0.03	0.03	1101	1
southern Canadian Rockies	87013-27	2890	60	250	19	1098.4	0.8	0.1754	0.0006	32000	2000	9.45	0.03	0.03	9.45	0.03	0.03	1128	1
southern Canadian Rockies	80023	3750	70	6240	130	14.8	0.7	0.5708	0.0017	5443	15	89.90	0.45	0.45	89.85	0.46	0.46	19	1
southern Canadian Rockies	74008	1860	40	1660	30	404.3	0.7	1.447	0.004	25830	60	312.7	4.1	4.2	312.7	4.1	4.2	977	11
southern Canadian Rockies	68006	76	2	1954	40	57.4	0.9	1.0258	0.0055	634	4	333	11	12	332	11	11	147	5
southern Canadian Rockies	74005	1244	25	104445	2118	118.0	2.0	1.1311	0.0034	214	1	399	13	15	397	13	15	362	16

southern Canadian Rockies	68004	93	2	17281	348	46.5	1.2	1.0456	0.0050	89	0	441	26	32	436	27	31	159	14
southern Canadian Rockies	71034	4062	81	21850	442	26.0	2.4	1.0183	0.0048	3006	15	444	29	43	444	29	43	91	13
southern Canadian Rockies	70004-19	56.4	1.1	6640	130	33.2	1.7	1.033	0.004	139.4	0.6	477	31	45	473	31	45	126	15
southern Canadian Rockies	70004-133	123	2	2400	50	24.4	1.2	1.027	0.003	836	2	540	40	68	539	40	68	112	19
southern Canadian Rockies	71006x	1991	40	350	20	336.3	1.7	1.4555	0.0059	131491	6884	501	26	34	501	26	34	1380	120
southern Canadian Rockies	68003	86	2	947	19	38.8	1.1	1.0441	0.0035	1504	6	505	32	45	505	33	45	161	19
southern Canadian Rockies	70001-3	178	4	3910	80	13.4	1	1.009	0.003	732	1.8	507	32	46	506	32	46	56	8
southern Canadian Rockies	86004	215	4	2191	44	620.1	2.6	1.8597	0.0062	2899	11	540	26	34	540	26	33	2850	240
southern Canadian Rockies	ENF-1	324	6	35000	700	275.7	1.2	1.379	0.005	202.5	0.6	540	40	40	540	40	40	1280	130
southern Canadian Rockies	87005	321	6	1647	33	324.8	1.9	1.4492	0.0053	4478	18	555	36	51	555	36	51	1560	200
southern Canadian Rockies	68001	59	1	4376	88	104.2	1.6	1.1402	0.0047	242	1	557	50	85	556	51	84	500	100
southern Canadian Rockies	71035	2140	43	5474	111	125.0	2.0	1.1764	0.0058	7302	43				>600				
southern Canadian Rockies	72050	102	2	651	13	436.8	1.6	1.6204	0.0057	4045	18				>600				
southern Canadian Rockies	87015	1105	22	2218	46	120.7	2.0	1.1730	0.0044	9282	59				>600				
southern Canadian Rockies	71041	3820	80	3250	70	9.3	0.7	1.01	0.002	18870	40				>600				

southern Canadian Rockies	73008	2250	40	2000	40	9.5	1.2	1.011	0.003	18060	50				>600				
Nahanni	GV-a	1788	36	732	15	-3.5	0.5	0.9691	0.0012	37584	115	396.9	7	7.6	396.9	7.1	7.6	-11	2
Nahanni	GV-a	2071	41	65	79	-5.1	1.8	0.9673	0.0030	487829	592463	398	16	18	398	16	18	-16	6
Nahanni	GV-a-50	1560	30	640	30	1.6	1.0	0.9720	0.0030	37500	1400	382	12	13	382	12	13	5	3
Nahanni	GV-a-132	2140	40	500	20	1.7	0.9	0.9740	0.0030	66000	3000	389	12	14	389	12	14	5	3
Nahanni	73055-A14	1683	34	4784	135	228.1	1.6	1.2772	0.0051	7134	145	398	13	14	398	13	14	701	28
Nahanni	73055-A14	986	20	3254	66	202.7	0.5	1.2504	0.0034	6015	22	418	10	12	417	10	12	658	20
Nahanni	73055-A14-36	4240	80	78100	1600	171.7	1.0	1.2230	0.0030	1056	5	475	17	19	474	17	19	655	33
Nahanni	73055-A14-62	3700	70	1480	30	10.4	0.6	1.0100	0.0030	40000	300	582	57	113	582	57	113	54	14
Nahanni	75037-C	4358	87	1150	23	-17.6	0.9	0.9518	0.0013	57284	186	403.4	9.1	10	403.4	9.1	10	-55	3
Nahanni	73059	12996	260	113	2	53.7	0.4	1.0502	0.0015	1910488	8875	416.8	7.9	8.4	416.8	8	8.5	174	4
Nahanni	73059-56	9850	200	42	9	71.8	0.7	1.0740	0.0030	4000000	900000	415	12	14	415	12	14	232	9
Nahanni	73059-78	9140	180	830	18	72.8	0.9	1.0740	0.0030	187800	1800	410	12	14	410	12	14	231	9
Nahanni	75037-B	3690	74	156	3	-32.6	0.7	0.9334	0.0016	350753	2193	412	11	12	412	11	12	-104	4
Nahanni	75037-A-2	3759	75	22	0	-19.2	0.6	0.9679	0.0014	2638199	8956	576	38	61	576	38	61	-98	15
Nahanni	75037-A-11	4736	95	10	0	-13.0	0.6	0.9777	0.0012	7059807	58337	606	44	83	606	44	83	-72	14
Nahanni	72034	9257	185	-33	-56	12.8	1.5	1.0875	0.0025	4000000	2000000				>600				
Nahanni	72034-28	3532	71	685	14	12.7	1.4	1.0256	0.0026	83924	570				>600				
Nahanni	73051	3113	62	23265	470	9.9	2.2	1.0147	0.0029	2155	8				>600				
Nahanni	73051	8008	169	714	14	7.5	0.4	1.0143	0.0015	180505	152				>600				
Nahanni	73052	7374	148	5131	103	0.2	1.0	0.9988	0.0014	22793	22				>600				
Nahanni	72BL-2	6608	136	7245	147	37.6	0.7	1.0548	0.0019	15274	53				>600				
Nahanni	73055-A15	9951	199	834	17	25.3	1.2	1.0377	0.0024	196501	323				>600				
northern Yukon	BC-C1-P2	275	6	6660	140	17.7	1.0	0.9098	0.0028	597	3	240.5	2.9	3	239.8	3.2	2.7	35	2

northern Yukon	BC-EPR-P1	449	9	485	10	0.0	0.6	0.9746	0.0051	14343	80	401	20	24	400	20	25	0.0	2.0
northern Yukon	BC-EPR-P1-10	378	8	39.4	1.4	1.4	1.2	0.997	0.003	152000	5000	542	64	150	541	68	150	10	11
northern Yukon	CP-89-31	123	2	4119	85	16.2	1.1	1.0149	0.0021	481	3	532	32	45	531	32	45	72.0	9.0
northern Yukon	CP-89-31-3	138	3	10740	215	33.3	1.3	1.0252	0.003	208.8	0.5	428	16	19	426	16	20	111	7
northern Yukon	BC-32G	160	3	19384	393	53.9	0.8	1.0555	0.0048	139	1	441	23	29	438	25	27	185	14
northern Yukon	GDM-B-4	164	3	16680	335	35.9	1.5	1.0389	0.0047	162	1	495	38	59	492	38	60	144	21
northern Yukon	GDM-B-33	224	4	2680	50	5.7	0.7	0.9989	0.0035	1326	5	513	37	57	513	37	56	24	5
northern Yukon	GDM-B-64	228	5	4400	90	6.9	0.8	1.0002	0.0026	822	2	510	29	40	509	29	39	29	4
northern Yukon	BC-28	86	2	2461	51	9.3	1.0	1.0021	0.0052	559	4	494	43	71	493	43	71	37.0	7.0
northern Yukon	BC-28-13	86	2	6987	143	27.3	2.4	1.0238	0.0107	201	2				>600				
northern Yukon	CP-89-33	246	5	5964	120	3.0	1.0	1.0001	0.0024	656	1	597	58	120	597	59	120	16.0	7.0
northern Yukon	CP-89-33-3	247	5	1571	32	4.7	0.9	0.9959	0.0035	2487	9	496	33	48	496	33	48	19	4
northern Yukon	BC-C-5	205	4	2992	65	27.5	2.0	1.0283	0.0045	1120	10	504	43	71	504	43	71	114	21
northern Yukon	BC-B-3	177	4	325	8	3.8	1.6	0.9973	0.0030	8647	111	527	42	70	527	41	70	17.0	8.0
northern Yukon	BC-B-6	553	11	1308	39	-0.6	2.3	0.9974	0.0043	6694	151				>600				
northern Yukon	BC-B-11	198	4	46	1	2.0	2.0	0.9967	0.0030	68700	500	557	60	136	557	62	134	9	12
northern Yukon	BC-B-55	134	3	75	2	3.5	1.4	0.9956	0.0030	28100	200	510	35	52	510	35	52	15	6
northern Yukon	GDM-A	205	4	26295	532	23.6	0.9	1.0339	0.0052	128	1				>600				
northern Yukon	GDM-A-4	203	4	29254	590	30.1	1.9	1.0343	0.0050	114	1	530	54	109	526	56	107	133	33
northern Yukon	BC-24i	332	7	4049	82	16.4	1.1	1.0149	0.0039	1322	5	528	44	73	528	44	72	72	13
northern Yukon	BC-EPR-A	266	5	3534	71	9.5	0.4	1.3950	0.0057	1667	6				>600				
northern Yukon	BC-EPR-A-2	182	4	1880	40	6.3	0.9	1.0025	0.0029	1546	7	552	45	76	551	45	76	30	7

northern Yukon	CP-89-26-4	137	3	12300	200	21.6	1.2	1.03	0.004	181.4	0.7				>600				
northern Yukon	CP-89-26-17	164	3	5220	110	12.0	0.8	1.0125	0.0025	504	4	590	52	99	589	52	98	63	15
northern Yukon	TTH-B-20	3068	61	3064	61	0.1	0.7	0.9961	0.0012	15839	11	601	42	63	601	42	63	1	4
northern Yukon	BC-41-4	496	10	547	11	6.7	0.9	1.0073	0.0020	14500	90				>600				
northern Yukon	CP-89-08-6	2944	59	7159	143	2.4	1.7	1.0335	0.0025	6747	7				>600				
northern Yukon	CP-89-09-5	116	2	3962	80	2.7	2.1	1.1729	0.0033	544	2				>600				
northern Yukon	CP-89-10	147	3	1079	22	2.0	1.3	1.0218	0.0036	2211	13				>600				
northern Yukon	CP-89-11	1186	24	137632	2788	-7.3	1.0	1.0173	0.0045	139	1				>600				
northern Yukon	CP-89-17-3	2771	55	13233	265	1.2	1.5	1.0158	0.0031	3377	9				>600				
northern Yukon	CP-89-19	817	16	2588	52	3.1	0.8	1.0033	0.0038	5029	21				>600				
northern Yukon	CP-89-20-7	503	10	71200	1400	15.1	1.4	1.0463	0.0032	117.2	0.3				>600				
northern Yukon	CP-89-21	582	12	106147	2139	31.2	1.4	1.0537	0.0048	92	0				>600				
northern Yukon	CP-89-22-3	3116	62	19417	389	0.9	1.4	1.0119	0.001	2579	3				>600				
northern Yukon	CP-89-24-3	226	5	43692	882	40.7	1.7	1.0990	0.0054	90.2	0.5				>600				
northern Yukon	CP-89-25-5	287	6	12954	260	14.4	2	1.014	0.0066	357	2				>600				
northern Yukon	CP-89-28	255	5	20252	406	13.0	0.9	1.0340	0.0017	207	0				>600				
northern Yukon	CP-89-30-8	127	3	3208	65	3.1	1.8	1.0275	0.0061	645	4				>600				
northern Yukon	P13	110	2	2210	45	8.2	1.2	1.0097	0.0037	800	4				>600				
northern Yukon	P21-4	571	11	16710	335	1.5	1.8	1.0174	0.0040	552	2				>600				

[a]Reported errors for ^{238}U and ^{232}Th concentrations are estimated to be ±1% due to uncertainties in spike concentration; analytical uncertainties are smaller.

[b] $\delta^{234}U = ([^{234}U/^{238}U]_{activity} - 1) \times 1000$.

[c]$[^{230}Th/^{238}U]_{activity} = 1 - e^{-l230T} + (\delta^{234}U_{measured}/1000)[l230/(l230 - l234)](1 - e^{-(l230 - l234)} T)$, where T is the age. "Uncorrected" indicates that no correction has been made for initial ^{230}Th.

[d] Ages are corrected for detrital ^{230}Th assuming an initial $^{230}Th/^{232}Th$ of $(4.4\pm2.2) \times 10^{-6}$.

[e] $\delta^{234}U_{initial}$ corrected was calculated based on ^{230}Th age (T), i.e., $\delta^{234}U_{initial} = \delta^{234}U_{measured} \times e^{l234*T}$, and T is corrected age.

[f] B.P. stands for “Before Present” where the “Present” is defined as the January 1, 1950 C.E.

Decay constants for ^{230}Th and ^{234}U are from Cheng et al. (2013); decay constant for ^{238}U is 1.55125×10^{-10} yr-1 (Jaffey et al., 1971).

Supplementary References

Allen, J. L. and B. Sorbel (2008), Assessing the differenced Normalized Burn Ratio's ability to map burn severity in the boreal forest and tundra ecosystems of Alaska's national parks, Int. J. Wildland Fire, 17(4), 463-475.

Atkinson, T., P. Smart, and T. Wigley (1983), Climate and natural radon levels in Castleguard cave, Columbia Icefields, Alberta, Canada, Arct. Alp. Res., 487-502.

Brook, A. G. (1976), Geomorphology of the north karst, south Nahanni River region, Northwest Territories, Canada.

Daum, D. W. (1994), Fisheries Investigations on the Kandik, Charley, Nation, and Tatonduk Rivers, Yukon-Charley Rivers National Preserve, 1987 and 1988, US Fish and Wildlife Service, Fairbanks Fishery Resource Office.

Environmental Canada (2017), Canadian Climate Normals 1981-2010, Canada Atmospheric and Environment Service, Minister of Supply and Services Canada, Ottawa, Ontatio, Canada.

Ford, D. (1973), Development of the canyons of the South Nahanni River, NWT, Canadian Journal of Earth Sciences, 10(3), 366-378.

Ford, D. (2009), The South Nahanni: high-latitude limestone landscapes, in Geomorphological Landscapes of the World, , edited by Anonymous , pp. 13-20, Springer.

Ford, D. C. (1976), Evidences of multiple glaciation in South Nahanni National Park, Mackenzie Mountains, Northwest Territories, Canadian Journal of Earth Sciences, 13(10), 1433-1445.

Ford, D. C. (1993), Karst in cold environments, Canada's cold environments, McGill Quenn's Univ Press, Montreal, 199-222.

Gascoyne, M. and D. Nelson (1983), Growth mechanisms of recent speleothems from Castleguard Cave, Columbia Icefields, Alberta, Canada, inferred from a comparison of uranium-series and carbon-14 age data, Arct. Alp. Res., 537-542.

Harington, C. (2011), Quaternary cave faunas of Canada: a review of the vertebrate remains, J. Cave Karst Stud., 73(3), 162-180.

Harris, S. A. (1979), Ice Caves and Permafrost Zones in Southwest Alberta (Eishöhlen und Permafrost in Südwest-Alberta), Erdkunde, 61-70.

Harris, S. A. and D. E. Pedersen (1998), Thermal regimes beneath coarse blocky materials, Permafrost Periglacial Processes, 9(2), 107-120.

Harris, S. A. and R. J. E. Brown (1978), Plateau Mountain: A case study of alpine permafrost in the Canadian Rocky Mountains.

Hughes, O. L. (1972), Surficial geology of northern Yukon Territory and northwestern district of Mackenzie, Northwest Territories, Department of Energy, Mines and Resources.

Jaffey, A., K. Flynn, L. Glendenin, W. t. Bentley, and A. Essling (1971), Precision measurement of half-lives and specific activities of U 235 and U 238, Physical Review C, 4(5), 1889.

Lauriol, B., L. Carrier, and P. Thibaudeau (1988), Topoclimatic zones and ice dynamics in the caves of the Northern Yukon, Canada, Arctic, 215-220.

Lauriol, B., C. Prévost, É. Deschamps, J. Cinq-Mars, and S. Labrecque (2001), Faunal and archaeological remains as evidence of climate change in freezing caverns, Yukon Territory, Canada, Arctic, 135-141.

Lauriol, B., C. Prévost, and D. Lacelle (2006), The distribution of diatom flora in ice caves of the northern Yukon Territory, Canada: relationship to air circulation and freezing, International Journal of Speleology, 35(2), 4.

Lauriol, B. (2016), The Ni'iinlii Njik Caves, Northern Yukon: Notes on Geology and History, edited by H. Leduc, Government of Yukon.

Marshall, P. and M. Brown (1974), Ice in Coulthard Cave, Alberta, Canadian Journal of Earth Sciences, 11(4), 510-518.

Norris, D. (1978), Geological maps of Yukon territory and northwest territories: Geol, Survey of Can., Open-File Rept., OF, 78(499), 6.

Parker, C. L. and D. F. Murray (1995), Status and Trends Survey of Category 2 Plants in the Yukon-Charley Rivers National Preserve, Alaska, University of Alaska Museum, Herbarium.

Rollins, J. (2004), Caves of the Canadian Rockies and the Columbia Mountains, Rocky Mountain Books Ltd.

Yonge, C., D. Ford, G. Horne, B. Lauriol, and J. Schroeder, Ice Caves in Canada, *In Press.*

Zazula, G. D., A. Duk-Rodkin, C. E. Schweger, and R. E. Morlan (2004), Late Pleistocene chronology of glacial Lake Old Crow and the north-west margin of the Laurentide Ice Sheet, Developments in Quaternary Sciences, 2, 347-362.Barker, S., D. Archer, L. Booth, H. Elderfield, J. Henderiks, and R. E. Rickaby (2006), Globally increased pelagic carbonate production during the Mid-Brunhes dissolution interval and the CO 2 paradox of MIS 11, Quaternary Science Reviews, 25(23), 3278-3293.